



Article

Topological Refraction in Kagome Split-Ring Photonic Insulators

Huichang Li ¹ , Chen Luo ¹, Tailin Zhang ¹, Jianwei Xu ¹, Xiang Zhou ¹, Yun Shen ^{1,*} and Xiaohua Deng ^{1,2,*}

¹ School of Physics and Materials Science, Nanchang University, Nanchang 330031, China; lhc_qx@163.com (H.L.); nc_lc@email.ncu.edu.cn (C.L.); 400603420025@email.ncu.edu.cn (T.Z.); xjw799576510@163.com (J.X.); zx610080@163.com (X.Z.)

² Institute of Space Science and Technology, Nanchang University, Nanchang 330031, China

* Correspondence: shenyun@ncu.edu.cn (Y.S.); dengxiaohua0@gmail.com (X.D.)

Abstract: A valley-Hall-like photonic insulator based on C_{3v} Kagome split-ring is proposed. Theoretical analysis and numerical calculations illustrate that C_{3v} symmetry can be broken not only by global rotation α but also individual rotation θ of the split rings, providing topological phase transitions. Furthermore, refraction of the edge state from the interface into the background space at Zigzag termination is explored. It is shown that positive/negative refraction of the outgoing beam depends on the type of valley (K or K'), from which the edge state is projected. These results provide a new way to manipulate terahertz wave propagation and facilitate the potential applications in directional collimation, beam splitting, negative refraction image, etc.

Keywords: topological phase transition; valley-Hall-like topology; edge states; topological refraction



Citation: Li, H.C.; Luo, C.; Zhang, T.L.; Xu, J.W.; Zhou, X.; Shen, Y.; Deng, X.H. Topological Refraction in Kagome Split-Ring Photonic Insulators. *Nanomaterials* **2022**, *12*, 1493. <https://doi.org/10.3390/nano12091493>

Academic Editor: Onofrio M. Marago

Received: 7 March 2022

Accepted: 31 March 2022

Published: 28 April 2022

Publisher's Note: MDPI stays neutral with regard to jurisdictional claims in published maps and institutional affiliations.



Copyright: © 2022 by the authors. Licensee MDPI, Basel, Switzerland. This article is an open access article distributed under the terms and conditions of the Creative Commons Attribution (CC BY) license (<https://creativecommons.org/licenses/by/4.0/>).

1. Introduction

Photonic topological insulators support some of the most fascinating properties for signal transport and show excellent potential applications in modern optical devices [1–7], such as reflectionless waveguides, topological quantum interfaces, splitters, robust delay lines, etc.

The key to topological phase transition lies in opening an energy gap in the band structure at certain degenerate points by breaking either the time-reversal symmetry (TRS) or inversion symmetry, which can be realized in classical wave systems mimicking the quantum Hall effect (QHE) [8–14], the quantum spin Hall effect (QSHE) [15–23], or the quantum valley Hall effect (QVHE) [24–33]. In analogues of the QHE system, breaking of TRS can be achieved by applying a magnetic field or an effective ‘magnetic’ field from circulating fluid flows [10–12] or gyroscopes [13,14]. However, this strategy remains challenging due to the structural complexity. In mimicking QSHE or QVHE systems, breaking the symmetry does not require any external fields. Generally, analogues of QSHE can be provided by constructing the system to have two pseudospins, either integrating the different wave polarization degree of freedom or folding the band structure to form a double Dirac cone [15–23,30]. For emulating QVHE, such as C_{3v} symmetry photonic crystals composed of triangular rods [6,24,34], square lattices containing square inclusions [35], the new class of valley-Hall-like topological insulators can be designed by breaking the inversion symmetry of the systems [36–38].

So far, varieties of topological insulators have been demonstrated. However, most of the current studies focus on the robust wave propagation along the topological interfaces [10–14,31,32,39–41]. Further exploration for applicable topological devices, including outcoupling effects or wave manipulations, need to be taken into consideration. More recently, topological positive/negative, near-zero refraction and wave splitting have been reported in valley crystal [25,29–31], Weyl [42], and QSHE inspired systems [43,44], which

may have potential applications in directional collimation [45], beam splitting [46–48], and others.

In this work, a new kind of valley-Hall-like photonic insulator based on two-dimensional (2D) C_{3v} Kagome split-ring is proposed. Theoretical analysis and numerical calculations by COMSOL Multiphysics illustrate that C_{3v} symmetry can be broken not only by global rotation α but also by individual rotation θ of the split rings, providing topological phase transitions. Further, topological positive/negative refraction of the edge states from the interface into background space at Zigzag termination is explored. The results show that refraction of the outgoing beam depends on the type of valley (K or K') from which the edge state is projected.

2. Model and Calculation Method

2.1. Model

The 2D unit cell of C_{3v} Kagome split-ring photonic insulator (SRPI) is shown in Figure 1a, where the lattice constant, and the inner and outer diameters of each split ring are a , r_1 , and r_2 , respectively. The background material is silicon (Si) with permittivity $\varepsilon = 11.7$, and the split ring is set as a perfect electric conductor. The proposed C_{3v} symmetry-broken unit cell to provide non-trivial valley-Hall-like topological states is demonstrated in Figure 1b, in which α and θ are the global and individual rotation of the split rings. As $a = 400 \mu\text{m}$, $r_1 = 0.1a$, $r_2 = 0.16a$, the photonic bands (TM modes with magnetic field along z axis) for $\alpha = 0^\circ, \theta = 0^\circ$, and $\alpha = 30^\circ, \theta = 0^\circ$ are shown in Figure 1c with blue and red curves, respectively. The existing bandgap closes for $\alpha = 0^\circ$ and opens for $\alpha = 30^\circ$.

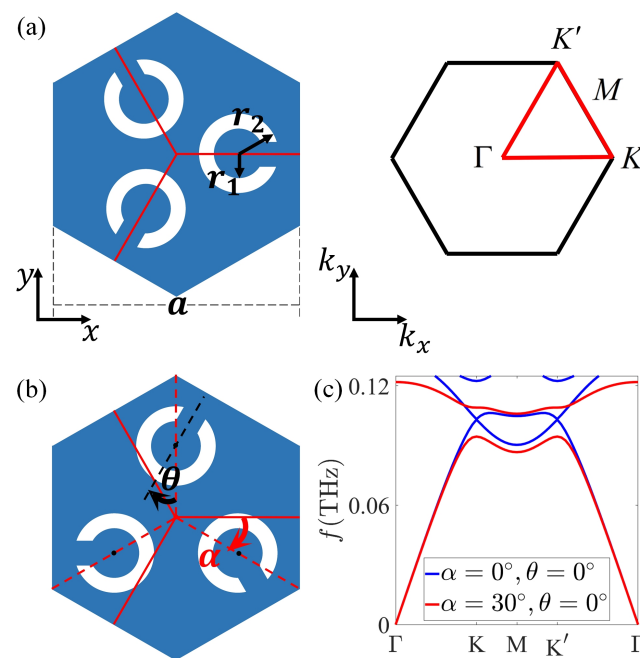


Figure 1. (a) The 2D unit cell and first Brillouin zone of C_{3v} Kagome SRPI. The geometric parameters are taken as $a = 400 \mu\text{m}$, $r_1 = 0.1a$, $r_2 = 0.16a$. (b) C_{3v} symmetry-broken unit cell, α and θ are the global and individual rotation of the split rings. (c) Photonic bands of the SRPI for $\alpha = 0^\circ, \theta = 0^\circ$ (blue solid curves) and $\alpha = 30^\circ, \theta = 0^\circ$ (red solid curves).

2.2. Valley Chern Number

In SRPI, the Dirac cone near the K point can be approximately regarded as a two-band model, and its effective Hamiltonian has the following form through the $\mathbf{k} \cdot \mathbf{p}$ perturbation method [24,49,50]:

$$H_K(\delta\mathbf{k}) = v_D(\delta k_x \sigma_x + \delta k_y \sigma_y) + m v_D^2 \sigma_z \quad (1)$$

where v_D is the group velocity at the degenerate Dirac cone, $\delta\mathbf{k}$ represents the momentum deviation from the K point, σ is Pauli matrix, $m = \pi(f_1 - f_2)/v_D^2$, f_1 and f_2 separately represent the two frequencies at the boundaries of bandgap after the Dirac point lifted. The Berry curvature can be obtained through effective Hamiltonian [49,51]:

$$\Omega(\delta\mathbf{k}) = \frac{mv_D}{2(\delta\mathbf{k}^2 + m^2v_D^2)^{\frac{3}{2}}} \quad (2)$$

The valley Chern number can be obtained by the numerical integration of Berry curvature around the K valley:

$$C_K = \frac{1}{2\pi} \int \Omega(\delta\mathbf{k}) dk^2 = \frac{\text{sgn}[m]}{2} = \frac{\text{sgn}(f_1 - f_2)}{2} \quad (3)$$

Equation (3) shows that the valley Chern number only depends on the sign of the Dirac mass m ($C_K = \frac{1}{2}$ for $m > 0$ and $C_K = -\frac{1}{2}$ for $m < 0$). The band inversion means the reversal of f_1 and f_2 , and consequently the signs of valley Chern number C_K .

3. Results

3.1. Band Inversion of Topological Valley-Hall-like States

Typically, the process of band inversion can make the bandgap open then close and then reopen, resulting in the topological phase transition at the K (or K') point [52]. For our proposed Kagome split-ring photonic insulator shown in Figure 1b, the topological phase transition depending on both global α and individual θ rotation is illustrated in Appendix A. Specifically, for $\theta = 0^\circ$, the topological phase varying with global α is shown in Figure 2a, in which the original C_{3v} symmetry at $\alpha = 0^\circ$ is reduced to the C_3 symmetry. Accordingly, the twofold Dirac degeneracy at the K (or K') point is lifted. The field distributions of the two eigenstates at the K point (denoted as p and q) for $\alpha = -30^\circ$ and 30° , respectively, are illustrated in Figure 2b. When the degeneracy is lifted, the frequency order of the p and q states flips, indicating a typical band inversion and topological phase transition. According to Equation (3), the signs of Dirac mass m ($\text{sgn}[m] = \text{sgn}[f_p - f_q]$) for bandgap I and II in Figure 2a are opposite, and the difference of valley Chern number I and II is $|\Delta C| = |C_K^I - C_K^{II}| = |\frac{1}{2} - (-\frac{1}{2})| = 1$, which implies that valley-Hall-like topological edge states can exist at the interface of system composed of SRPIs with distinct valley-Hall-like phases (Section 3.2).

As $\alpha = 30^\circ$, the topological phase varying with global θ is shown in Figure 2c. The field profiles of the eigenstates at the K point for $\theta = -180^\circ, -110^\circ, -70^\circ$, and 0° are shown in Figure 2d. Similar to Figure 2b, the frequency order of the eigenstates flips for different θ . With two different bands in Figure 2b involved in the topological phase transition, three bands are involved in Figure 2c, where two different kinds of band inversions (one is between III (III) and IV (VI), and the other is between IV (VI) and V (V)) exist. In regions III (III) and IV (VI), the signs of Dirac mass m ($\text{sgn}[m] = \text{sgn}[f_s - f_q]$) are opposite, and the difference of their valley Chern numbers is $|\Delta C| = |C_K^{III} - C_K^{IV}| = |-\frac{1}{2} - \frac{1}{2}| = 1$, which guarantees the existence of topological edge states (Appendix B). Similarly, for IV (VI) and V (V), opposite signs of Dirac mass m ($\text{sgn}[m] = \text{sgn}[f_p - f_q]$) and different valley Chern numbers ($|\Delta C| = |C_K^{IV} - C_K^V| = |\frac{1}{2} - (-\frac{1}{2})| = 1$) are obtained, providing topological edge states (Appendix B).

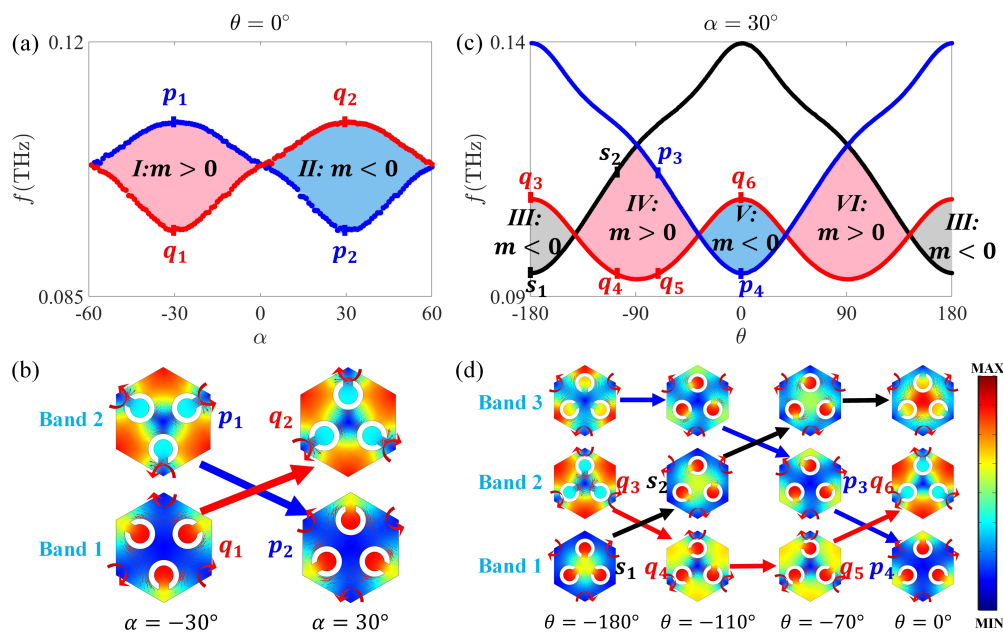


Figure 2. (a) Dependence of topological phase transition on global α as $\theta = 0^\circ$ at the K point; the region I and II represent bandgaps with $m > 0$ and $m < 0$, respectively. (b) The field distribution of the two eigenstates at the K point (denoted as p and q) for $\alpha = -30^\circ$ and 30° . (c) Dependence of topological phase transition on individual θ as $\alpha = 30^\circ$ at the K point; the region III, IV (VI) and V represent bandgaps with $m < 0$, $m > 0$, and $m < 0$, respectively. (d) The field distribution of three eigenstates at the K point (denoted as s , p , and q) for $\theta = -180^\circ$, -110° , -70° , and 0° . The Poynting vectors are represented by red arrows.

3.2. Valley Topological Refraction

It is known that the direction of the outgoing beam of the topological edge state depends on the type of valley (K or K'), from which the edge state is projected [45]. Hence, a wave launched from left to right along positive-type and negative-type interfaces will be projected from the K and K' valley, respectively. To illustrate the refraction of the radiated beam, a topological insulator in Figure 3a is designed, and refractions of edge states from the interface into the background space at Zigzag termination are explored.

Figure 3b shows the dispersion relation of the topological insulator containing different interfaces. Dashed black curves represent the bulk modes, and the dashed red/blue curves represent the negative-type/positive-type interfaces edge states. For different points at the interfaces edge states, the distributions of fields and Poynting vectors (represented by arrows) are shown in Figure 3c.

The k -space analysis on out-coupling of K projected edge states along the positive-type (Zigzag) interface is demonstrated in Figure 4a. The white solid hexagon represents the first Brillouin zone, and red solid circles show the dispersion in background material Si, in which the incident wavevector K will be matched with the equifrequency curve of Si to determine the propagation direction of the radiated beam. The simulated distribution of fields at frequency $f = 0.102$ THz is illustrated in the bottom panel. For out-coupling of K' projected edge state along the negative-type (Zigzag) interface, the corresponding analyses are shown in Figure 4b. Obviously, the direction of the outgoing beam in Figure 4a is different with that in Figure 4b due to the different type of valley (K or K') from which the edge state is projected. Further, the theoretical refraction angle can be quantitatively determined by the phase-matching condition $k \cdot e_{term} = K \cdot e_{term}$ at the terminal (parallel to e_{term}), which is $|k| \cdot \cos(60^\circ - \theta_{rK}) = |K| \cdot \cos 60^\circ$ and $|k| \cdot \cos(120^\circ + \theta_{rK'}) = |K| \cdot \cos 60^\circ$, for positive-type and negative-type interfaces, respectively. Here, the equifrequency curves k of background Si can be determined by $|k| = 2\pi \cdot \frac{f \cdot n_{Si}}{c}$, where f represents the incident frequency, c is light speed in air, and $n_{Si} = 3.42$ is the refractive index of Si. Consequently,

$\theta_{rK} = 15.78^\circ$ and $\theta_{rK'} = -75.78^\circ$ are obtained in Figure 4a,b. We note that the topological refraction and transmission in our SRPI can maintain strong robustness (Appendix C).

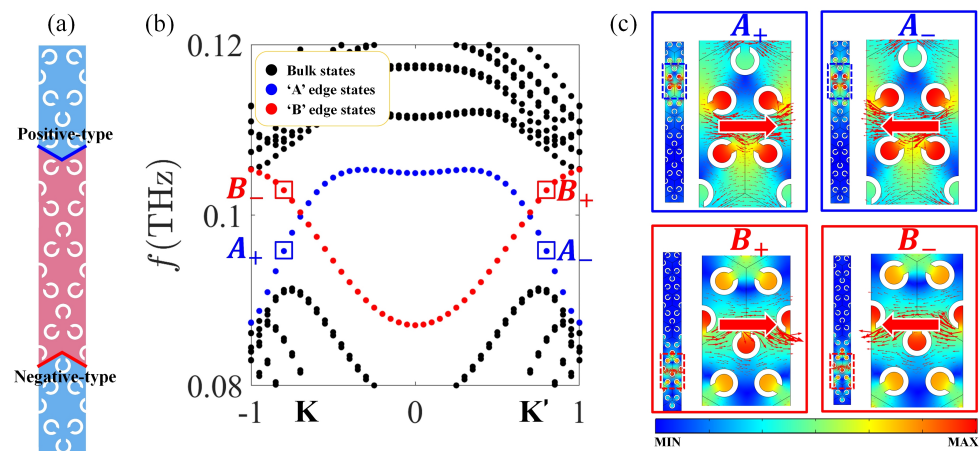


Figure 3. (a) Supercell and (b) bands of topological insulator with $\alpha = -30^\circ, \theta = 0^\circ$ (light red) and $\alpha = 30^\circ, \theta = 0^\circ$ (light blue). In (b), dashed black curves represent the bulk modes and the dashed red/blue curves represent the negative-type/positive-type interfaces edge states. (c) The distribution of field for A_+, A_-, B_+, B_- in (b), and the Poynting vectors are represented by red arrows.

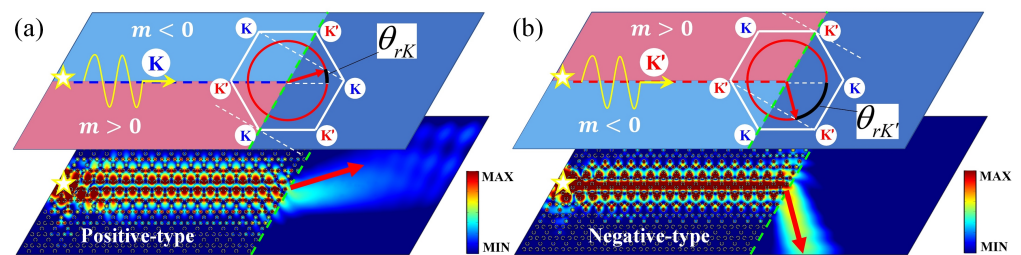


Figure 4. (a) The k -space analysis on out-coupling of K valley projected edge states along the positive-type (Zigzag) interface. (b) The k -space analysis on the out-coupling of K' valley projected edge states along the negative-type (Zigzag) interface. The white solid hexagon represents the first Brillouin zone, and the red solid circles show the dispersion in background material Si. The simulated distribution of fields at the frequency $f = 0.102$ THz (in bandgap) are separately illustrated in the bottom panels. The light-red and light-blue regions represent $m > 0$ and $m < 0$, respectively.

4. Conclusions

A valley-Hall-like photonic insulator based on C_{3v} Kagome split-ring is proposed. Theoretical analysis and numerical calculations illustrate that C_{3v} symmetry can be broken by either the global rotation α or individual rotation θ of split rings, providing topological phase transitions. Additionally, refractions of the outgoing beam from the interface into the background space at Zigzag termination are explored. We show that positive/negative refraction can be obtained, which is determined by the type of valley (K or K'). These results provide a new way to manipulate THz wave propagation and facilitate the potential applications in directional collimation, beam splitting, and negative refraction image.

Author Contributions: Y.S. and X.D. supervised this project. H.L. provided the original idea and did the calculations. H.L., C.L., T.Z., J.X., X.Z. and Y.S. analyzed the data and discussed the results. H.L. and Y.S. wrote the paper. All authors have read and agreed to the published version of the manuscript.

Funding: The authors are grateful for the support from the National Natural Science Foundation of China (Grant numbers 61865009, 61927813).

Data Availability Statement: The data presented in this study are available on request from the corresponding author.

Conflicts of Interest: The authors declare no conflict of interest.

Appendix A

Topological phase transition at the K point depending on global α and individual θ rotation is illustrated in Figure A1.

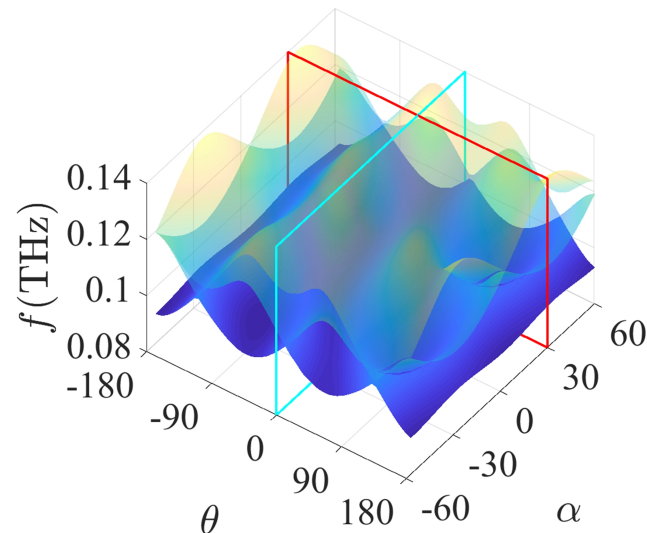


Figure A1. Dependence of topological phase transition at K point on global α and individual θ rotations. Specifically, the cross sections formed by the cyan frame and the red frame are shown in Figure 2a,c.

Appendix B

For the band inversion between bandgap III and IV , the corresponding supercell, bands, and k -space analysis are shown in Figure A2a–c, respectively. Nonzero $|\Delta C|$ supports the existence of negative-type/positive-type topological edge states. Specifically, for negative refraction, $\theta_{rK'_1} = -76.96^\circ$ is obtained.

For IV and V , supercell, bands, and k -space analysis are separately shown in Figure A2d–f. Likewise, nonzero $|\Delta C|$ supports the existence of negative-type/positive-type topological edge states, and the corresponding negative refraction angle is $\theta_{rK'_2} = -76.37^\circ$.

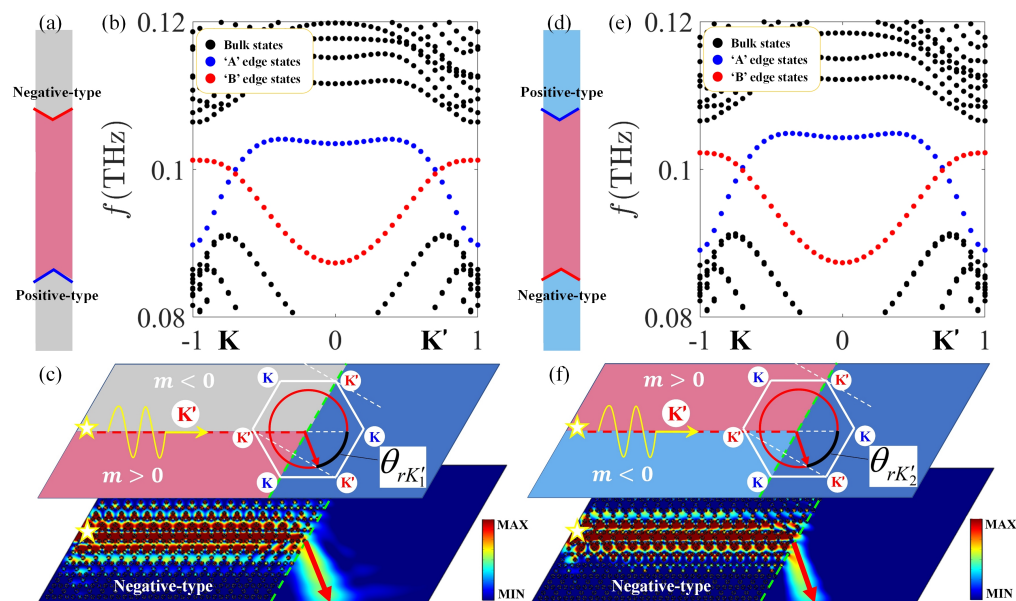


Figure A2. (a) Supercell and (b) bands of topological insulator with $\alpha = 30^\circ, \theta = -180^\circ$ (gray) and $\alpha = 30^\circ, \theta = -110^\circ$ (light red). (c) The k -space analysis on the out-coupling of K' valley and projected edge states along negative-type (Zigzag) interface. (d) Supercell and (e) bands of topological insulator with $\alpha = 30^\circ, \theta = -70^\circ$ (light red) and $\alpha = 30^\circ, \theta = 0^\circ$ (light blue). (f) The k -space analysis on the out-coupling of K' valley and projected edge states along negative-type (Zigzag) interface. In (b,e), dashed black curves represent the bulk modes. The dashed red/blue curves represent the negative-type/positive-type interfaces edge states. In (c,f), the white solid hexagon represents the first Brillouin zone. The red solid circle shows the dispersion in background material Si. Simulated distribution of fields at frequency $f = 0.1$ THz and $f = 0.101$ THz are separately illustrated in the bottom panels.

Appendix C

By adding impurity and defect, topological refraction and transmission can maintain strong robustness, as shown in Figure A3.

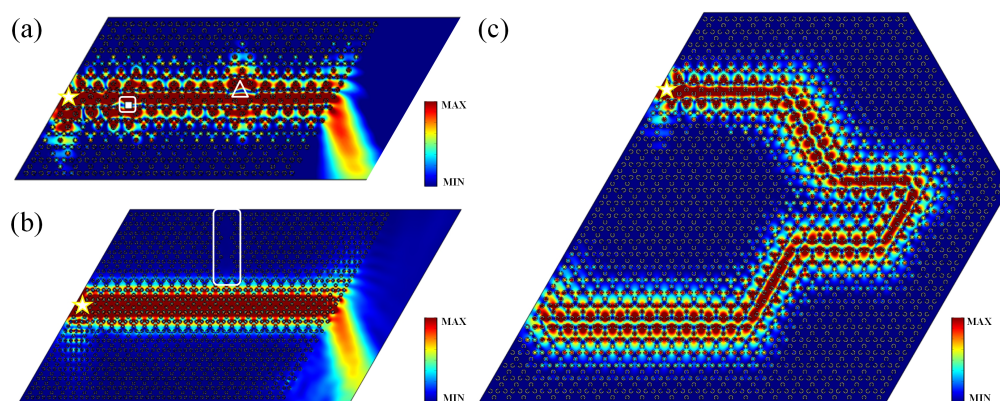


Figure A3. Simulated propagation of a light beam through the Zigzag interface with $f = 0.102$ THz. In (a), the tentagram, square, and triangle represent source, impurity, and defect, respectively. In (b), the tentagram and rectangle represent source and defect, respectively. In (c), the tentagram represents source.

References

1. Rycerz, A.; Tworzydło, J.; Beenakker, C.W.J. Valley filter and valley valve in graphene. *Nat. Phys.* **2007**, *3*, 172–175. [[CrossRef](#)]
2. Xiao, D.; Yao, W.; Niu, Q. Valley-contrasting physics in graphene: Magnetic moment and topological transport. *Phys. Rev. Lett.* **2007**, *99*, 236809. [[CrossRef](#)] [[PubMed](#)]
3. Garcia-Pomar, J.L.; Cortijo, A.; Nieto-Vesperinas, M. Fully valley-polarized electron beams in graphene. *Phys. Rev. Lett.* **2008**, *100*, 236801. [[CrossRef](#)] [[PubMed](#)]
4. Hafezi, M.; Demler, E. A.; Lukin, M. D.; Taylor, J. M. Robust optical delay lines with topological protection. *Nat. Phys.* **2011**, *7*, 907–912. [[CrossRef](#)]
5. Lai, K.; Ma, T.; Bo, X.; Anlage, S.; Shvets, G. Experimental realization of a reflections-free compact delay line based on a photonic topological insulator. *Sci. Rep.* **2016**, *6*, 28453. [[CrossRef](#)]
6. Zhang, Z.W.; Tian, Y.; Cheng, Y.; Wei, Q.; Liu, X.J.; Christensen, J. Topological acoustic delay line. *Phys. Rev. Appl.* **2018**, *9*, 034032. [[CrossRef](#)]
7. Kang, Y.H.; Ni, X.; Cheng, X.J.; Khanikaev, A.B.; Genack, A.Z. Pseudo-spin–valley coupled edge states in a photonic topological insulator. *Nat. Commun.* **2018**, *9*, 3029. [[CrossRef](#)]
8. Haldane, F.D.M.; Raghun, S. Possible realization of directional optical waveguides in photonic crystals with broken time-reversal symmetry. *Phys. Rev. Lett.* **2008**, *100*, 013904. [[CrossRef](#)]
9. Lu, L.; Joannopoulos, J.D.; Soljačić, M. Topological photonics. *Nat. Photonics* **2014**, *8*, 821–829. [[CrossRef](#)]
10. Khanikaev, A.B.; Fleury, R.; Mousavi, S.H.; Alu, A. Topologically robust sound propagation in an angular-momentum-biased graphene-like resonator lattice. *Nat. Commun.* **2015**, *6*, 8260. [[CrossRef](#)]
11. Wang, P.; Lu, L.; Bertoldi, K. Topological phononic crystals with one-way elastic edge waves. *Phys. Rev. Lett.* **2015**, *115*, 104302. [[CrossRef](#)] [[PubMed](#)]
12. Nash, L.M.; Kleckner, D.; Read, A.; Vitelli, V.; Turner, A.M.; Irvine, W.T.M. Topological mechanics of gyroscopic metamaterials. *Proc. Natl. Acad. Sci. USA* **2015**, *112*, 14495. [[CrossRef](#)] [[PubMed](#)]
13. Yang, Z.; Gao, F.; Shi, X.; Lin, X.; Gao, Z.; Chong, Y.; Zhang, B. Topological Acoustics. *Phys. Rev. Lett.* **2015**, *114*, 114301. [[CrossRef](#)] [[PubMed](#)]
14. Ding, Y.; Peng, Y.; Zhu, Y.; Fan, X.; Yang, J.; Liang, B.; Zhu, X.; Wan, X.; Cheng, J. Experimental demonstration of acoustic chern insulators. *Phys. Rev. Lett.* **2019**, *122*, 014302. [[CrossRef](#)] [[PubMed](#)]
15. Mousavi, S.H.; Khanikaev, A.B.; Wang, Z. Topologically protected elastic waves in phononic metamaterials. *Nat. Commun.* **2015**, *6*, 8682. [[CrossRef](#)]
16. Mei, J.; Chen, Z.; Wu, Y. Pseudo-time-reversal symmetry and topological edge states in two-dimensional acoustic crystals. *Sci. Rep.* **2016**, *6*, 32752. [[CrossRef](#)] [[PubMed](#)]
17. He, C.; Ni, X.; Ge, H.; Sun, X.C.; Chen, Y.B.; Lu, M.H.; Liu, X.P.; Chen, Y.F. Acoustic topological insulator and robust one-way sound transport. *Nat. Phys.* **2016**, *12*, 1124–1129. [[CrossRef](#)]
18. Xia, B.Z.; Liu, T.T.; Huang, G.L.; Dai, H.Q.; Jiao, J.R.; Zang, X.G.; Yu, D.J.; Zheng, S.J.; Liu, J. Topological phononic insulator with robust pseudospin-dependent transport. *Phys. Rev. B* **2017**, *96*, 094106. [[CrossRef](#)]
19. Yves, S.; Fleury, R.; Lemoult, F.; Fink, M.; Lerosey, G. Topological acoustic polaritons: Robust sound manipulation at the subwavelength scale. *New J. Phys.* **2017**, *19*, 075003. [[CrossRef](#)]
20. Miniaci, M.; Pal, R.K.; Morvan, B.; Ruzzene, M. Experimental Observation of Topologically Protected Helical Edge Modes in Patterned Elastic Plates. *Phys. Rev. X* **2018**, *8*, 031074. [[CrossRef](#)]
21. Yang, L.; Yu, K.; Wu, Y.; Zhao, R.; Liu, S. Topological spin-hall edge states of flexural wave in perforated metamaterial plates. *J. Phys. D* **2018**, *51*, 325302. [[CrossRef](#)]
22. Yu, S.Y.; He, C.; Wang, Z.; Liu, F.K.; Sun, X. C.; Li, Z.; Lu, H.Z.; Lu, M.H.; Liu, X.P.; Chen, Y.F. Elastic pseudospin transport for integratable topological phononic circuits. *Nat. Commun.* **2018**, *9*, 3072. [[CrossRef](#)] [[PubMed](#)]
23. Chaunsali, R.; Chen, C.W.; Yang, J. Subwavelength and directional control of flexural waves in zone-folding induced topological plates. *Phys. Rev. B* **2018**, *97*, 054307. [[CrossRef](#)]
24. Lu, J.; Qiu, C.; Ye, L.; Fan, X.; Ke, M.; Zhang, F.; Liu, Z. Observation of topological valley transport of sound in sonic crystals. *Nat. Phys.* **2017**, *13*, 369–374. [[CrossRef](#)]
25. Gao, F.; Xue, H.; Yang, Z.; Lai, K.; Yu, Y.; Lin, X.; Chong, Y.; Shvets, G.; Zhang, B. Topologically protected refraction of robust kink states in valley photonic crystals. *Nat. Phys.* **2018**, *14*, 140–144. [[CrossRef](#)]
26. Makwana, M.P.; Craster, R.V. Geometrically navigating topological plate modes around gentle and sharp bends. *Phys. Rev. B* **2018**, *98*, 184105. [[CrossRef](#)]
27. Wu, Y.; Chaunsali, R.; Yasuda, H.; Yu, K.; Yang, J. Dial-in topological metamaterials based on bistable stewart platform. *Sci. Rep.* **2018**, *8*, 112. [[CrossRef](#)]
28. Wang, W.; Bonello, B.; Djafari-Rouhani, B.; Pennec, Y. Topological valley, pseudospin, and pseudospin-valley protected edge states in symmetric pillared phononic crystals. *Phys. Rev. B* **2019**, *100*, 140101(R). [[CrossRef](#)]
29. Zhu, Z.; Huang, X.; Lu, J.; Yan, M.; Li, F.; Deng, W.; Liu, Z. Negative refraction and partition in acoustic valley materials of a square lattice. *Phys. Rev. Appl.* **2019**, *12*, 024007. [[CrossRef](#)]
30. Xie, B.; Liu, H.; Cheng, H.; Liu, Z.; Chen, S.; Tian, J. Acoustic topological transport and refraction in a kekulé lattice. *Phys. Rev. Appl.* **2019**, *11*, 044086. [[CrossRef](#)]

31. Wang, W.; Bonello, B.; Djafari-Rouhani, B.; Pennec, Y. Polarization-dependent and valley-protected Lamb waves in asymmetric pillared phononic crystals. *J. Phys. D* **2019**, *52*, 505302. [[CrossRef](#)]
32. Zheng, L.Y.; Achilleos, V.; Chen, Z.G.; Richoux, O.; Theocharis, G.; Wu, Y.; Mei, J.; Felix, S.; Tournat, V.; Pagneux, V. Acoustic graphene network loaded with helmholtz resonators: A first-principle modeling, dirac cones, edge and interface waves. *New J. Phys.* **2020**, *22*, 013029. [[CrossRef](#)]
33. Zhang, Q.; Chen, Y.; Zhang, K.; Hu, G. Dirac degeneracy and elastic topological valley modes induced by local resonant states. *Phys. Rev. B* **2020**, *101*, 014101. [[CrossRef](#)]
34. Lu, J.; Qiu, C.; Deng, W.; Huang, X.; Li, F.; Zhang, F.; Chen, S.; Liu, Z. Valley topological phases in bilayer sonic crystals. *Phys. Rev. Lett.* **2018**, *120*, 116802. [[CrossRef](#)] [[PubMed](#)]
35. Xia, B.Z.; Zheng, S.J.; Liu, T.T.; Jiao, J.R.; Chen, N.; Dai, H.Q.; Yu, D.J.; Liu, J. Observation of valleylike edge states of sound at a momentum away from the high-symmetry points. *Phys. Rev. B* **2018**, *97*, 155124. [[CrossRef](#)]
36. Lu, J.; Qiu, C.; Ke, M.; Liu, Z. Valley vortex states in sonic crystals. *Phys. Rev. Lett.* **2016**, *116*, 093901. [[CrossRef](#)]
37. Wu, X.; Meng, Y.; Tian, J.; Huang, Y.; Xiang, H.; Han, D.; Wen, W. Direct observation of valley-polarized topological edge states in designer surface plasmon crystals. *Nat. Commun.* **2017**, *8*, 1304. [[CrossRef](#)]
38. Raj K.P.; Massimo, R. Edge waves in plates with resonators: An elastic analogue of the quantum valley Hall effect. *New J. Phys.* **2017**, *19*, 025001.
39. Miniaci, M.; Pal, R.K.; Manna, R.; Ruzzene, M. Valley-based splitting of topologically protected helical waves in elastic plates. *Phys. Rev. B* **2019**, *100*, 024304. [[CrossRef](#)]
40. Wang, W.; Jin, Y.; Wang, W.; Bonello, B.; Djafari-Rouhani, B.; Fleury, R. Robust Fano resonance in a topological mechanical beam. *Phys. Rev. B* **2020**, *101*, 024101. [[CrossRef](#)]
41. Zheng, L.Y.; Christensen, J. Topological radiation engineering in hyperbolic sonic semimetals. *Phys. Rev. B* **2021**, *103*, 064307. [[CrossRef](#)]
42. He, H.; Qiu, C.; Ye, L.; Cai, X.; Fan, X.; Ke, M.; Zhang, F.; Liu, Z. Topological negative refraction of surface acoustic waves in a Weyl phononic crystal. *Nat. (London)* **2018**, *560*, 61–64. [[CrossRef](#)] [[PubMed](#)]
43. Zhang, Z.; Tian, Y.; Cheng, Y.; Liu, X.; Christensen, J. Experimental verification of acoustic pseudospin multipoles in a symmetry-broken snowflakelike topological insulator. *Phys. Rev. B* **2017**, *96*, 241306(R). [[CrossRef](#)]
44. Huang, H.; Tan, Z.; Huo, S.; Feng, L.; Chen, J.; Han, X. Topologically protected zero refraction of elastic waves in pseudospin-hall phononic crystals. *Commun. Phys.* **2020**, *3*, 46. [[CrossRef](#)]
45. Zhang, Z.; Tian, Y.; Wang, Y.; Gao, S.; Cheng, Y.; Liu, X.; Christensen, J. Directional acoustic antennas based on valley-hall topological insulators. *Adv. Mater.* **2018**, *30*, 1803229. [[CrossRef](#)]
46. Ju, L.; Shi, Z.; Nair, N.; Lv, Y.; Jin, C.; Velasco, J.; Ojeda-Aristizabal, J.C.; Bechtel, H.A.; Martin, M.C.; Zettl, A.; Analytis, J.; Wang, F. Topological valley transport at bilayer graphene. *Nature* **2015**, *520*, 650–655. [[CrossRef](#)]
47. Li, J.; Wang, K.; McFaul, K.J.; Zern, Z.; Ren, Y.; Watanabe, K.; Taniguchi, T.; Qiao, Z.; Zhu, J. Gate-controlled topological conducting channels in bilayer graphene. *Nat. Nanotech.* **2016**, *11*, 1060–1065. [[CrossRef](#)]
48. Li, J.; Zhang, R.X.; Yin, Z.; Zhang, J.; Watanabe, K.; Taniguchi, T.; Liu, C.; Zhu, J. A valley valve and electron beam splitter. *Science* **2018**, *362*, 1149–1152. [[CrossRef](#)]
49. Wang, Z.Y.; Yang, Y.Z.; Li, H.Y.; Jia, H.; Luo, J.L.; Huang, J.; Wang, Z.N.; Jiang, B.; Yang, N.J.; Jin, G.J.; Yang, H. Multichannel Topological Transport in an Acoustic Valley Hall Insulator. *Phys. Rev. Appl.* **2021**, *15*, 024019. [[CrossRef](#)]
50. Chen, Y.; He, X.T.; Cheng, Y.J.; Qiu, H.Y.; Feng, L.T.; Zhang, M.; Dai, D.X.; Guo, G.C.; Dong, J.W.; Ren, X.F. Topologically Protected Valley-Dependent Quantum Photonic Circuits. *Phys. Rev. Lett.* **2021**, *126*, 230503. [[CrossRef](#)]
51. Jia, D.; Ge, Y.; Xue, H.R.; Yuan, S.Q.; Sun, H.X.; Yang, Y.H.; Liu, X.J.; Zhang, B.L. Topological refraction in dual-band valley sonic crystals. *Phys. Rev. B* **2021**, *103*, 144309. [[CrossRef](#)]
52. Zhang, X.J.; Liu, L.; Lu, M.H.; Chen, Y.F. Valley-Selective Topological Corner States in Sonic Crystals. *Phys. Rev. Lett.* **2021**, *126*, 156401. [[CrossRef](#)] [[PubMed](#)]